NSRRC-Jo 4713 (2015)

Soft Matter

PAPER

View Article Online
View Journal | View Issue

Published on 16 April 2015. Downloaded by National Center for High-Performance Computing on 15/05/2015 02:18:35.

Cite this: *Soft Matter*, 2015, 11, 4041

Differential dependencies on $[Ca^{2+}]$ and temperature of the monolayer spontaneous curvatures of DOPE, DOPA and cardiolipin: effects of modulating the strength of the inter-headgroup repulsion†

Y.-F. Chen,* K.-Y. Tsang, W.-F. Chang and Z.-A. Fan

Received 10th March 2015,
Accepted 16th April 2015

DOI: 10.1039/c5sm00577a

www.rsc.org/softmatter

Biomembranes assume nonlamellar structures in many cellular events, with the tendency of forming a nonlamellar structure quantified by the monolayer spontaneous curvature, C_0, and with many of these events involving the acts of Ca^{2+}. Despite this biologically important intimacy, how C_0 is affected by $[Ca^{2+}]$ is unknown. In this study, we use the X-ray diffraction technique and the reconstruction of electron density profiles to measure the C_0s of a zwitterionic phospholipid, DOPE, and two anionic phospholipids, DOPA and 18:1 (9Z) cardiolipin, at temperatures from 20 °C to 40 °C and $[Ca^{2+}]$s from 0 mM to 100 mM; these phospholipids are chosen to examine the contributions of the electric charge density per molecule. While showing a strong dependence on temperature, $C_{0,DOPE}$ is nearly independent of $[Ca^{2+}]$. In contrast, $C_{0,DOPA}$ and $C_{0,cardiolipin}$ are almost unresponsive to the temperature change but affected by the $[Ca^{2+}]$ variation; and $C_{0,DOPA}$ varies with $[Ca^{2+}]$ ~1.5 times more strongly than $C_{0,cardiolipin}$, with the phase preferences of DOPA and cardiolipin shifting to the H_{II} phase and remaining on the L_α phase, respectively, at $[Ca^{2+}]$ = 100 mM. From these observations, we reveal the effects of modulating the strength of the inter-headgroup repulsion and discuss the mechanisms underlying the phase behaviour and cellular functions of the investigated phospholipids. Most importantly, this study recognizes that the headgroup charge density is dominant in dictating the phase behaviour of the anionic phospholipids, and that the unique molecular characteristics of cardiolipin are critically needed both for maintaining the structural integrity of cardiolipin-rich biomembranes and for fulfilling the biological roles of the phospholipid.

Introduction

The conspicuous role played by phospholipids in constituting biomembranes may belie the structural diversity displayed by their self-assembled aggregates. In fact, even biomembranes assume nonlamellar structures during the courses of many biological events, such as exocytosis and viral invasion.[1,2] Among the diverse phospholipid components of a biomembrane, some species display higher propensities of nonlamellar structure formation than others when they are dispersed in water alone. These differential nonlamellar-forming tendencies have long been explained with the relaxed molecular shape of a phospholipid (*i.e.*, the shape assumed by a phospholipid molecule when it is free of any constraint). Optimally, a phospholipid self-assembles into a supramolecular structure that reflects the relaxed shape of its molecule under given conditions (Fig. 1a). The relaxed molecular shape of a phospholipid may vary with the environmental conditions; elevating temperature, for example, can enhance the splaying of the hydrocarbon chains of a phospholipid and thus drive its relaxed molecular shape to grow more conical.[3,4]

The essence of the shape concept can be captured and quantified with monolayer spontaneous curvature, C_0, which describes the monolayer curvature of the optimal supramolecular structure reflecting the relaxed molecular shape of a given phospholipid. The larger the magnitude of its C_0, the more the phospholipid is inclined to adopt nonlamellar structures or the more the structure formed by the phospholipid is curved; and the positive and negative C_0s indicate the preference of the phospholipid to the type I and type II structures, respectively (Fig. 1a). C_0 also varies with the environmental conditions. The C_0s of several phospholipids were shown to exhibit clear dependencies on temperature,[3] on the condition of the aqueous medium[5] and presumably on hydrostatic pressure.[6,7] When the phospholipids with different C_0s are mixed, the resulting supramolecular structure would

Department of Chemical and Materials Engineering, National Central University, Taoyuan 32001, Taiwan. E-mail: yifanchen@ncu.edu.tw

† Electronic supplementary information (ESI) available: Structural parameters of the phospholipid mixtures and the statistical method of uncertainty estimation for a linear fitting. See DOI: 10.1039/c5sm00577a

Published on 16 April 2015. Downloaded by National Center for High-Performance Computing on 15/05/2015 02:18:35.

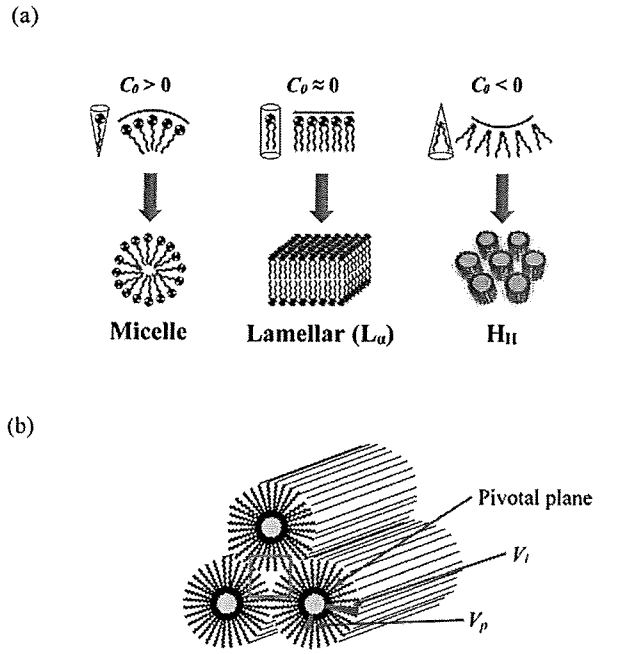

Fig. 1 (a) Correlation among C_0, the relaxed molecular shape and preferred supramolecular structure of a phospholipid. Within each phospholipid cylinder of the H_{II} phase is the cylindrical core of water. (b) An energetically forbidden interstice (red box) would be formed in the hydrocarbon chain region of a type II structure if the optimal length of the tails and the uniformity of the interfacial curvature are maintained simultaneously. The position of the pivotal plane and the definitions of V_p and V_i for the H_{II} phase are also marked (see text).

optimally exhibit a collective C_0 weighted by the relative amounts of the composing phospholipids.

The presence in the lamellar biomembranes of the phospholipids with $C_0 \neq 0$ is said to maintain, within the biomembranes, an elastic stress (the elastic stress per unit area, $g_E = \frac{1}{2}K(C - C_0)^2 + K_G G$, where K and K_G are the bending and Gaussian moduli, and C and G are the total and Gaussian curvatures, respectively, of a monolayer)[8,9] of a certain strength to regulate the conformations and functioning of membrane proteins.[8,10–12] Indeed, many proteins have been shown to demonstrate correlations between their functioning (*e.g.*, the conductance of an ion channel, alamethicin),[13] enzymatic activity (*e.g.*, the lipase activities of α-Toxin),[14] conformation (*e.g.*, the orientation of an amphiphilic peptide, MSI-103, in a membrane)[15] or protein–protein interactions (*e.g.*, the αβ-tubulin-induced blockage of the voltage-dependent anion channel)[16] with the collective C_0 of the biomembrane that hosts the proteins. Given this biological significance of C_0 regulation, investigating how C_0 is tuned by biologically important factors is of great value to understanding the cellular activities that involve nonlamellar biomembranes and the stored elastic stresses. Ca^{2+} participates in many cellular activities (*e.g.*, cellular signaling,[17] apoptosis[18] and mitochondrial energy metabolism[19,20]), and some of these activities are associated with the formation of nonlamellar biomembranes (*e.g.*, exocytosis)[21] and thus C_0. Despite this close tie between Ca^{2+} and C_0, how they interplay with each other is still unknown. In this study, we examine the correlation between C_0 and Ca^{2+} to explore the mechanisms underlying the related cellular activities.

To measure C_0, the phospholipid of interest must self-assemble under constraint-free conditions such that the resulting supramolecular structure exhibits a total curvature equivalent to the C_0. Following the well-adopted method developed by Rand, Gruner and co-workers,[22,23] the constraint-free conditions are attained here by adding free hydrocarbons (in this study, tetradecane) and excess water to the phospholipid suspensions. The free hydrocarbons relieve the packing frustration of the hydrocarbon chains, which occurs when phospholipid molecules are arranged into a type II structure[12,23] (see Fig. 1b), whereas the presence of excess water circumvents the constraint arising from the hydration repulsion.[24] Furthermore, if a phospholipid self-assembles into the H_{II} phase (a type II structure, see Fig. 1a), the radius of the water core of this structure can be directly converted to the C_0 by definition, provided this radius is determined by a structure-determination technique, such as X-ray diffraction. By employing this principle and the X-ray diffraction technique, we measure the C_0s of three important phospholipids, DOPE (known for forming the H_{II} phase preferentially), DOPA and 18 : 1 (9*Z*) cardiolipin, suspended in the buffered solutions (pH = 7.2) containing different $[Ca^{2+}]$s. Specifically, we aspire to understand how modulating the strength of the inter-headgroup electrostatic repulsion by varying $[Ca^{2+}]$ would affect the C_0s of three phospholipids which carry the same type of hydrocarbon chains (*i.e.*, the acyl chain with 18 carbons and 1 double bond at the C9 position, that is, 18 : 1 (9*Z*)) but differ in the number of the net electric charges on their headgroups (*i.e.*, cardiolipin carries two, DOPA one and DOPE no net negative charges per molecule). We expect that the knowledge learned here can be generalized to the cases where factors other than Ca^{2+} weaken the inter-headgroup repulsion; this repulsion is known to influence the phase behavior of anionic phospholipids (*i.e.*, the phospholipids carrying net negative charges, such as DOPA and cardiolipin) considerably.[25,26,68] The implications to the cation-induced $L_\alpha \rightarrow H_{II}$ transition for PE and to the phase behavior and cellular functions of DOPA and cardiolipin, particularly those concerning the PA involvement in the intracellular transport and the unique molecular characteristics of cardiolipin, are discussed.

Experimental

Sample preparation

Dioleoylphosphatidylethanolamine (DOPE, cat. no. 850725C), dioleoyl phosphatidic acid (DOPA, cat. no. 840875C) and 18 : 1 (9*Z*) cardiolipin (cat. no. 710335C; unless otherwise specified, all "cardiolipin" mentioned hereafter refers to this species) dissolved in chloroform were purchased from Avanti (Alabaster, AL) and used without further purification. These stock solutions were stored at −20 °C immediately after received and used within 6 months. The DOPE–DOPA (or DOPE–cardiolipin) mixture was prepared by mixing the DOPA (or cardiolipin) and DOPE stock

 This journal is © The Royal Society of Chemistry 2015

Published on 16 April 2015. Downloaded by National Center for High-Performance Computing on 15/05/2015 02:18:35.

solutions in a desired molar ratio. The mixed solution was dried under a gentle stream of argon gas, followed by an overnight vacuum incubation to remove the residual chloroform. The dried phospholipid film was re-dissolved in 2-methylbutane (cat. no. M32631, Sigma-Aldrich) after tetradecane (cat. no. 87140, Aldrich) was added to the films. The solution was vortexed vigorously to ensure the well mixing of the phospholipids and tetradecane. 2-Methylbutane was removed following the same procedure as for removing chloroform, with the vacuum incubation process carefully controlled such that the residual 2-methylbutane was evaporated before the escape of tetradecane. The dry film of phospholipid(*s*)-tetradecane was suspended in the excessive buffer solution (pH = 7.2) containing 10 mM HEPES (cat. no. H0887, Sigma-Aldrich) and calcium chloride (cat. no. C3306, Sigma) of a desired concentration. Each sample finally contained DOPE and DOPA (or cardiolipin) in a specified molar ratio, 16 wt% of tetradecane and excessive buffered aqueous solution containing $CaCl_2$ of a fixed concentration. Two-way centrifugation alternated with a vigorous vortex and >10 freeze–thaw cycles were carried out to homogenize the samples. The samples were allowed to equilibrate at 4 °C for 2–3 days before the collection of the X-ray diffraction data.

Data collection

The X-ray diffraction data were collected at Beamlines BL13A1 and BL23A1 of the National Synchrotron Radiation Research Center (NSRRC) in Hsinchu, Taiwan. BL13A1 and BL23A1 produced photons with the energies of 12 keV and 15 keV, and were equipped with a Mar165 CCD detector (pixel number = 1024 × 1024, active area = 61 × 61 mm^2) and a Pilatus3 1 M detector from DECTRIS (Baden, Switzerland), respectively. The sample-to-detector distance was calibrated with silver behenate.

Before the main data collection, each sample was subjected to a "homogeneity test," in which the X-ray beam was shot through different parts of the sample to examine the spatial variations of the diffraction pattern and peak position; any significant change in the diffraction pattern and peak position indicated the inhomogeneity of the sample and unqualified the sample for the main data collection. All the samples that proceeded to the main data collection phase displayed no spatial variation in the diffraction pattern and <0.4 Å variation in the peak position, which was considered as one of the sources of the uncertainty in measurement. In the main data collection, the samples, each with *a* fixed phospholipid composition and $[Ca^{2+}]$, experienced three temperatures (*i.e.*, 20 °C, 30 °C and 40 °C) in sequence at which the X-ray diffraction images were taken. 20 minute equilibrium time was applied to each of the temperature points before the samples were exposed to X-rays. In addition to the diffraction images of the samples, those of the buffer solutions and the empty sample cells were also recorded. The X-ray transmissions were also measured for the background subtraction purpose.

Data processing and the electron density profile reconstruction

The data collected at BL23A1 were reduced and azimuthally integrated with the in-house program of the beamline to produce the 1-D diffraction profiles (Fig. 2a), while the reduction

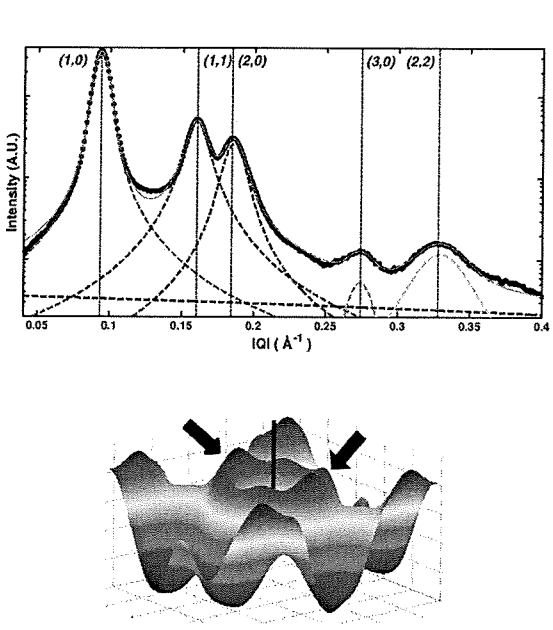

Fig. 2 (a) 1-D diffraction profile of a DOPE–DOPA mixture (10 mol% DOPA, $[Ca^{2+}]$ = 100 mM), fitted globally with the Voigt functions for the peaks and a linear function for the diffuse background. The orange solid line is the sum of the fitted functions, which agrees well with the data (solid dots). (b) Electron density profile of the H_{II} phase formed by a phospholipid. Surrounded by the electron-dense area (marked with arrows) is the cylindrical water core. The azimuthal average of the distances between the electron-density peaks and the axis of the water core (a vertical line) defines the radius of the water core, R_w.

and azimuthal integration of the data from BL13A1 were carried out with the program TVX (version 7.2, courtesy of Prof. Sol Gruner and Dr Mark Tate of Cornell University). The background scattering arising from the buffer solution and other scatterers (*e.g.*, air) on the flight path was subtracted from the 1-D diffraction profiles with the X-ray transmissions of the samples, buffer solutions and the empty sample cells taken into consideration. Only the diffraction patterns that indicated the sole presence of the H_{II} phase were used for further data processing (the sole presence of the H_{II} structure is the prerequisite for the method employed here to determine C_0); any hint of phase coexistence led to the removal of the data from further processing.

The processed 1-D diffraction profiles were used for the reconstruction of the electron density profiles. The diffraction profiles were fitted globally with the Voigt functions (the convolution of the Lorentz and Gaussian functions) for the peaks and with a linear function for the diffuse scattering (Fig. 2a) to extract the positions, $\vec{q}$ ($\vec{q} = 4\pi\sin\theta/\lambda$, where 2θ is the diffraction angle and λ is the X-ray wavelength), and intensities (the integrated areas under the peaks), I_q, of the Bragg peaks. The reconstruction was implemented in the Matlab environment and followed the concept developed in ref. 29, where the electron density, ρ_e, in a centrosymmetric unit cell (*e.g.*, the unit cell of the H_{II} phase) is expressed as,

$$\rho_e(\vec{r}) = \rho_{avg} + \sum_q A_q \cos(\vec{q}\cdot\vec{r}),$$

Published on 16 April 2015. Downloaded by National Center for High-Performance Computing on 15/05/2015 02:18:35.

where $\vec{r}$ is the position vector within the unit cell; ρ_{avg} is the average electron density; and A_q is related to I_q through,

$$A_q^2 \propto \frac{I_q \sin\theta}{m}, \quad (1)$$

where $\sin\theta \approx \theta$ (2θ is the diffraction angle) is the Lorentz correction and m is the multiplicity factor. (It should be noted that some studies employed $\sin 2\theta$ or θ^2 as the Lorentz correction. However, the Lorentz correction was $\sin\theta$ in our case, since the diffraction images had been azimuthally integrated.[27,28]) While the magnitude of A_q can be determined through eqn (1), its sign (*i.e.*, the phase of the diffracted X-ray) must be derived by other means. Here, we employed the phasing suggested in ref. 3 and 28 for the H_{II} phase: "+" for the (1,0) peak; "−" for (1,1); "−" for (2,0); "+" for (2,1); "+" for (3,0); "+" for (2,2); and "+" for (3,1). We also examined other phasing possibilities, but none could result in an electron density distribution compatible with the known structure of the H_{II} phase. Since only the relative electron density was relevant to our purpose, ρ_{avg} was not explicitly determined.

Once the electron density profile (as illustrated in Fig. 2b) is obtained, many structural parameters regarding the H_{II} phase are extractable, the most important of which in this study being the radius of the cylindrical water core, R_w, and the water volume fraction, ϕ_w, of the H_{II} unit cell. Following the convention (see, for example, ref. 29 and 30), R_w was defined as the azimuthally averaged distance between the axis of the water core and the maxima of the electron density, where the electron-dense phosphorous moieties of the headgroups resided (Fig. 2b). Based on the geometry of the H_{II} phase, R_w is correlated with ϕ_w through,[27]

$$\phi_w = \frac{2\pi R_w^2}{\sqrt{3}d^2}, \quad (2)$$

where d, the lattice spacing of the H_{II} unit cell, was experimentally determined from the diffraction data and R_w was obtained through the reconstruction. The d and R_w for all the samples examined in this study are summarized in Table S1 of the ESI.† These data were used to determine ϕ_w through eqn (2). The ϕ_w and R_w were then used to determine the radius of curvature against the pivotal plane. The detail is described below.

Position of the pivotal plane and determination of the radius of curvature

The pivotal plane is defined as a dividing surface within the phospholipid monolayer of the H_{II} phase (Fig. 1b), where the cross-sectional area of a phospholipid molecule remains constant upon isothermal bending.[22,32,33] Conventionally, C_0 is measured against this pivotal plane, rather than against the water–lipid interface, because such defined C_0 corresponds to the elastic stress consistent with those determined by other means.[22] The pivotal plane can be experimentally located through X-ray diffraction measurements for the variation of the H_{II} lattice spacing upon dehydration (*e.g.*, ref. 5, 31 and 35). The spontaneous radius of curvature against the pivotal plane, R_p (= $1/C_0$), can be obtained once the position of the plane is known. Based on the geometry of the H_{II} phase, a correlation between R_p and the other structural parameters is established,[31]

$$R_p = R_w\sqrt{1 + \frac{1-\phi_w}{\phi_w}\frac{V_p}{V_l}}, \quad (3)$$

where V_p is the volume within a phospholipid molecule enclosed between the water–lipid interface and the pivotal plane (Fig. 1b) and V_l is the molecular volume of the phospholipid. While ϕ_w, based on which the H_{II} lattice spacing can be converted to R_w through eqn (2), is a controlled variable in a dehydration experiment, the ratio of V_p/V_l, which dictates the position of the pivotal plane, must be determined through the relations,[31]

$$\frac{A_w^2}{V_l^2} = \frac{A_p^2}{V_l^2} - 2\frac{V_p}{V_l}\frac{A_w}{V_l R_w},$$

and

$$\frac{A_w}{V_l} = \frac{2\phi_w}{(1-\phi_w)R_w},$$

where A_w and A_p are the cross-sectional area per molecule at the water–lipid interface and at the pivotal plane, respectively. V_p/V_l can be derived from the slope of the straight line in the so-called diagnostic plot,[31,33] where A_w^2/V_l^2 is plotted against A_w/R_wV_l. Placing the obtained V_p/V_l along with the known ϕ_w and R_w into eqn (3) gives R_p.

Instead of carrying out the dehydration experiments and determining V_p/V_l experimentally, this present study located the pivotal plane for the samples of various compositions (DOPE, DOPE/DOPA and DOPE/cardiolipin in various molar ratios) and at different temperatures by exploiting two important findings from several seminal studies: first, V_p/V_l is independent of the composition of a phospholipid mixture, as long as DOPE is the dominant component (at least >70 mol% in the mixture); the DOPE–DOPA, DOPE–DOPS and DOPE–DOG (dioleoylglycerol) mixtures of various molar ratios exhibit the V_p/V_l values essentially identical to that of pure DOPE.[5,31,33] Second, V_p/V_l varies linearly with temperature,[32,35] allowing one to accurately estimate the V_p/V_l ratios at different temperatures once the V_p/V_l ratio at one temperature is known. Together with eqn (3) and the ϕ_w and R_w values determined as described in the previous sub-section, these findings have allowed us to calculate R_p for the DOPE–DOPA and DOPE–cardiolipin mixtures, as well as for pure DOPE, at various compositions and temperatures by adopting the V_p/V_l values summarized in ref. 32, ranging from V_p/V_l = 0.35 to 0.303 at temperatures from 20 °C to 40 °C. The results, expressed as $C_0 = 1/R_p$, are summarized in Table S1 of the ESI.† All the C_0s presented here are defined this way, with an exception of Table 1 and Table S1 of the ESI.† In these tables, the C_0s defined against the neutral plane (*i.e.*, a dividing surface within the monolayer where bending and stretching are energetically independent),[70] obtained following the method described in ref. 3, are also presented. This is to facilitate comparisons with the earlier studies where C_0 is defined against the neutral plane (*e.g.*, ref. 3). All the results and conclusions

 This journal is © The Royal Society of Chemistry 2015

Published on 16 April 2015. Downloaded by National Center for High-Performance Computing on 15/05/2015 02:18:35.

Table 1 The C_0s, in $Å^{-1}$, of DOPE, DOPA and 18 : 0 (9Z) cardiolipin at various temperatures and $[Ca^{2+}]$s. The uncertainty is intrinsic to a linear fitting and was determined according to the standard statistical principle described in the ESI. The values in the parentheses are the C_0s defined against the neutral plane (see text)

		$[Ca^{2+}]$					
Lipid		0 mM	10 mM	20 mM	50 mM	70 mM	100 mM
DOPE	20 °C	−0.0331 ± 0.0009 (−0.0388 ± 0.0008)	−0.0340 ± 0.0009 (−0.0399 ± 0.0008)	−0.0342 ± 0.0008 (−0.0397 ± 0.0008)	−0.0343 ± 0.0009 (−0.0406 ± 0.0008)	−0.0343 ± 0.0009 (−0.0406 ± 0.0008)	−0.0347 ± 0.0009 (−0.0398 ± 0.0008)
	30 °C	−0.0345 ± 0.0012 (−0.0399 ± 0.0009)	−0.0355 ± 0.0011 (−0.0410 ± 0.0009)	−0.0356 ± 0.0010 (−0.0409 ± 0.0008)	−0.0355 ± 0.0011 (−0.0415 ± 0.0009)	−0.0354 ± 0.0011 (−0.0414 ± 0.0009)	−0.0356 ± 0.0010 (−0.0402 ± 0.0008)
	40 °C	−0.0365 ± 0.0014 (−0.0412 ± 0.0011)	−0.0376 ± 0.0011 (−0.0424 ± 0.0009)	−0.0377 ± 0.0011 (−0.0422 ± 0.0009)	−0.0374 ± 0.0011 (−0.0427 ± 0.0009)	−0.0373 ± 0.0011 (−0.0426 ± 0.0009)	—
DOPA	20 °C	−0.0106 ± 0.0039 (−0.0108 ± 0.0057)	−0.0122 (−0.0195)	—	−0.0233 ± 0.0074 (−0.0273 ± 0.0096)	−0.0249 ± 0.0032 (−0.0299 ± 0.0033)	−0.0312 ± 0.0043 (−0.0384 ± 0.0108)
	30 °C	−0.0105 ± 0.0042 (−0.0110 ± 0.0046)	−0.0072 (−0.0138)	—	−0.0234 ± 0.0079 (0.0265 ± 0.0099)	−0.0252 ± 0.0028 (−0.0294 ± 0.0027)	−0.0304 ± 0.010 (−0.0381 ± 0.022)
	40 °C	−0.0109 ± 0.0060 (−0.0118 ± 0.0073)	−0.0043 (−0.0096)	—	−0.0231 ± 0.0088 (0.0253 ± 0.0106)	−0.0245 ± 0.0021 (−0.0268 ± 0.0084)	—
Cardiolipin	20 °C	2.7×10^{-4} ± 0.0066 (-9.7×10^{-5} ± 0.0113)	−0.0040 ± 0.0083 (−0.0033 ± 0.0103)	−0.0036 ± 0.0091 (−0.0032 ± 0.0105)	−0.0090 ± 0.0055 (−0.0076 ± 0.0089)	—	−0.0146 ± 0.0022 (−0.0186 ± 0.0032)
	30 °C	2.2×10^{-4} ± 0.0067 (−0.0004 ± 0.0104)	−0.0041 ± 0.0091 (−0.0039 ± 0.01)	−0.0027 ± 0.0106 (−0.0026 ± 0.0119)	−0.0089 ± 0.0063 (−0.0077 ± 0.0096)	—	−0.0158 ± 0.0020 (−0.0203 ± 0.004)
	40 °C	6.9×10^{-4} ± 0.0077 (−0.0002 ± 0.0109)	−0.0037 ± 0.0098 (−0.0036 ± 0.0102)	−0.0017 ± 0.0111 (−0.0018 ± 0.0116)	−0.0087 ± 0.0079 (−0.0078 ± 0.0109)	—	−0.0165 ± 0.0039 (−0.0186 ± 0.0053)

presented here are valid for both the C_0 definitions, for which the differences in value are small, as observed in ref. 33.

The C_0 measurements for lamellar-preferring phospholipids

The method we used to measure C_0s entailed the sole presence of the H_{II} structure under excess water conditions. Therefore, lamellar-preferring DOPA and cardiolipin must be framed into the H_{II} phase before their C_0s are measurable. This can be achieved with the technique pioneered by Rand's and Gruner's groups[5,22,31,33] and widely adopted by many others (*e.g.*, ref. 3, 36 and 37). In this technique, a small amount of the lamellar-favoring phospholipid are mixed with a H_{II}-favoring, "host" species (*e.g.*, DOPE) to form the H_{II} phase in excess water conditions, such that the collective C_0 of the mixture can be determined in the same way as for a pure H_{II}-forming phospholipid (see Introduction). A series of collective C_0s are obtained for the mixtures of varying guest-to-host molar ratios. By assuming that the collective C_0 of the mixture varies linearly with the molar ratio, one can determine the C_0 of the guest species through extrapolation of the established linear correlation to 100 mol% of the guest. The assumed linearity between the collective C_0 and molar ratio of the mixture was unambiguously reproduced in this study for both the DOPE–DOPA and DOPE–cardiolipin mixtures at various $[Ca^{2+}]$s (Fig. 3), showing good miscibility of the guest and host species and the applicability of this technique. It should be emphasized that one single sample contributed to only one data point in Fig. 3, which presents the C_0 variations at 20 °C, and at least two more samples with the same condition were prepared to repeat the measurement for the uncertainty estimation. Hence, a multitude of samples were prepared only to determine the C_0-molar ratio correlation for one $[Ca^{2+}]$ value (*i.e.*, a set of data points fitted with one dashed line in Fig. 3). The C_0-molar ratio correlations for 30 °C and 40 °C were also obtained from the same sets of samples, since the diffraction data for 20 °C, 30 °C and 40 °C were collected for each of the samples. Through the linear extrapolations for the data points similarly presented as those in Fig. 3, the C_0s of DOPA and cardiolipin at different $[Ca^{2+}]$s and temperatures were derived individually from these C_0-molar ratio correlations for their respective mixtures with DOPE. The results, along with the C_0s of DOPE, are summarized in Table 1.

Results

The temperature and $[Ca^{2+}]$ dependencies of the C_0 of DOPE

We first examine the C_0 of DOPE ($C_{0,DOPE}$) at varieties of temperatures and $[Ca^{2+}]$s. This serves to both understand how $C_{0,DOPE}$ is affected by the two factors and, through scrutinizing the consistency between this and earlier studies, to reassure the validity of our methodology and the reliability of our data. $C_{0,DOPE}$ obtained in this study is −0.0331 ± 0.0009 $Å^{-1}$ (= 1/(−30.2 ± 0.8) $Å^{-1}$) at 20 °C and $[Ca^{2+}]$ = 0 mM, which is in good agreement with the literature values (*e.g.*, $C_{0,DOPE}$ = 1/(−30) $Å^{-1}$ at 20 °C in ref. 31; = 1/(−29.4 ± 2) $Å^{-1}$ at 22 °C in ref. 34; = 1/(−31.5) $Å^{-1}$ at 22 °C in ref. 22). The temperature dependence of $C_{0,DOPE}$ at $[Ca^{2+}]$ = 0 mM, −0.00017 $Å^{-1}$ $°C^{-1}$ (Fig. 4), also conforms to the value, −0.00013 ± 0.00004 $Å^{-1}$ $°C^{-1}$, reported in ref. 3. The excellent consistencies between this and the previous studies reassure the reliability of our data.

In contrast to its clear dependence on temperature, $C_{0,DOPE}$ demonstrates a weak response to the $[Ca^{2+}]$ variation at all the studied temperatures (Fig. 5). Given the zwitterionic nature of DOPE, this insensitivity to the $[Ca^{2+}]$ change is within the expectation and likely to be correlated with the low binding affinity of Ca^{2+} to PE. Indeed, the Ca^{2+} binding affinity of DMPE (14 : 0 PE) is markedly lower, by orders of magnitude, than those

Published on 16 April 2015. Downloaded by National Center for High-Performance Computing on 15/05/2015 02:18:35.

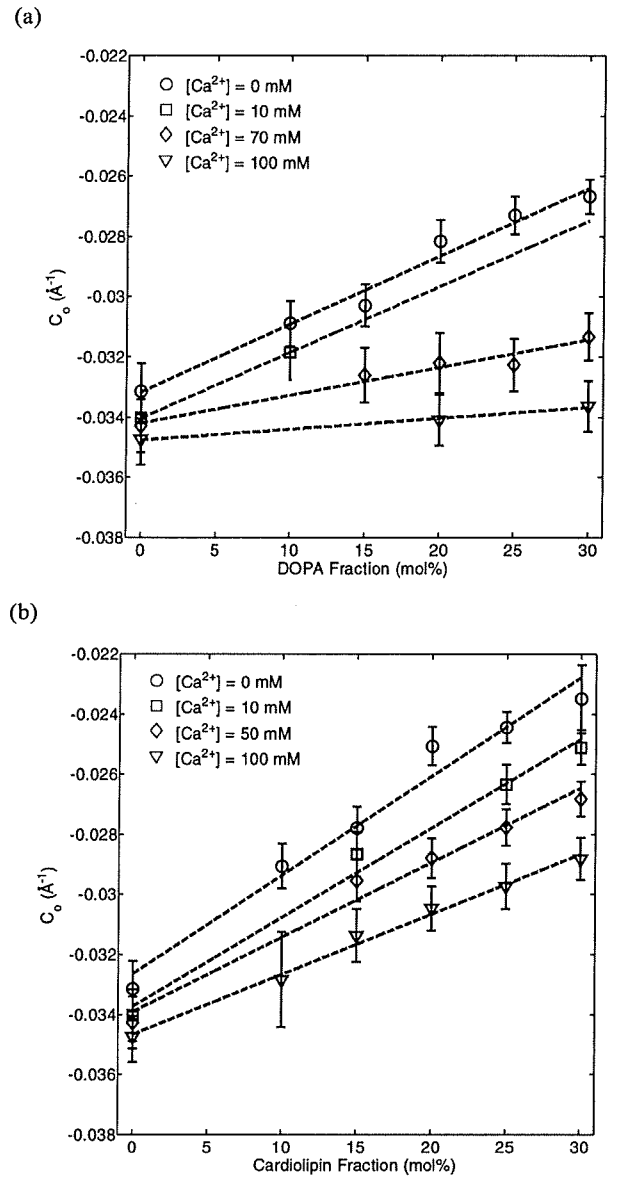

Fig. 3 The collective C_0 of the mixture as a function of the molar fraction of the guest species at 20 °C: (a) DOPE–DOPA and (b) DOPE–cardiolipin mixtures at different [Ca^{2+}]s. The dashed lines are linear fits to the sets of data points, which along with the corresponding data for other sample conditions yielded the C_0s of DOPA and cardiolipin presented in Fig. 4 and 5 and Table 1.

of several PC species, due to the reduced exposure of the main Ca^{2+} binding site (namely, the phosphate group) as a result of the hydrogen-bond network among PE molecules.[39]

The [Ca^{2+}] dependencies of the C_0s of DOPA and 18 : 1 (9*Z*) cardiolipin

The C_0s of DOPA and cardiolipin ($C_{0,DOPA}$ and $C_{0,cardiolipin}$, respectively) were measured at a variety of [Ca^{2+}]s to examine how modulating the strength of the inter-headgroup electrostatic repulsion would shift the phase preferences of the two

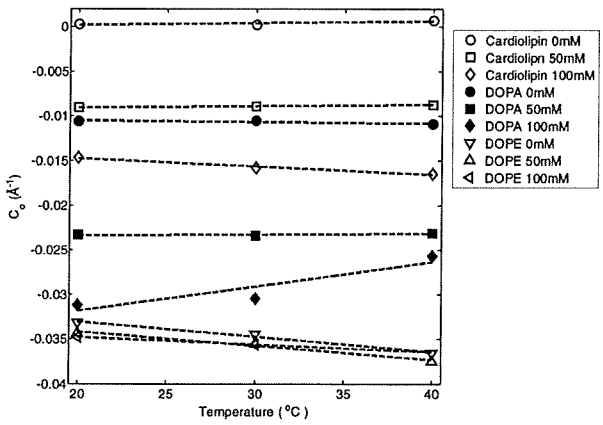

Fig. 4 $C_{0,DOPA}$, $C_{0,cardiolipin}$ and $C_{0,DOPE}$ as a function of temperature for different [Ca^{2+}]s. The dashed lines are linear fits to the sets of data points. The C_0s of DOPA and cardiolipin were determined through the linear extrapolations as depicted in Fig. 3.

anionic phospholipids (Fig. 5). The response of C_0 to the [Ca^{2+}] variation is far more pronounced for DOPA and cardiolipin than for DOPE: the spontaneous curvatures change from $C_{0,DOPA} = -0.0106 \pm 0.0039$ Å^{-1} (= 1/(−94.3) Å^{-1}) to $C_{0,DOPA} = -0.0312 \pm 0.0043$ Å^{-1} (= 1/(−32.1) Å^{-1}); and from $C_{0,cardiolipin} = +2.7 \times 10^{-4} \pm 0.0066$ Å^{-1} (= 1/(+3703.7) Å^{-1}) to $C_{0,cardiolipin} = -0.014 \pm 0.0022$ Å^{-1} (= 1/(−68.5) Å^{-1}) when [Ca^{2+}] is varied from 0 mM to 100 mM at 20 °C. (It is noted that the uncertainty is intrinsic to a linear fitting and does not arise from experimental errors; the uncertainty was estimated following the standard statistical principle described in the ESI.†) In contrast, the corresponding shift in $C_{0,DOPE}$ is merely a negligible one, from $C_{0,DOPE} = -0.0331 \pm 0.0009$ Å^{-1} (= 1/(−30.2) Å^{-1}) to $C_{0,DOPE} = -0.0347 \pm 0.0009$ Å^{-1} (= 1/(−28.8) Å^{-1}). The differential effects of Ca^{2+} on the C_0s of the anionic and zwitterionic phospholipids are presumably owing to the presence/absence of the net electric charges on the headgroups; screening the headgroup charges with Ca^{2+} is expected to weaken the inter-headgroup repulsions and drive the C_0s of the anionic phospholipids toward more negative values. Interestingly, $C_{0,DOPA}$ varies ~1.5 times more strongly with [Ca^{2+}] than $C_{0,cardiolipin}$ does (*i.e.*, 0.21 Å^{-1} M^{-1} for $C_{0,DOPA}$ *versus* 0.14 Å^{-1} M^{-1} for $C_{0,cardiolipin}$) (Fig. 5). Given the difference in the nominal charge density between the two phospholipids, this is not unforeseeable, as the [Ca^{2+}] needed for reducing the inter-headgroup repulsion to a certain degree may be nearly doubled for cardiolipin than for DOPA. In other words, the difference in charge density per molecule is likely to result in the differential responses to a stimuli of the same strength. The reason that the variation rates do not differ by an exact factor of two may lay on the differences in pK_a or in the binding affinity of Ca^{2+}. In this instance, the C_0 measurement is demonstrated to be an efficient way of quantifying a phenomenon that otherwise can afford a qualitative description only.

Upon changing [Ca^{2+}] from 0 mM to 100 mM at 20 °C, $C_{0,DOPA}$ shifts its value to 1/(−32.1) Å^{-1}, comparable to that of the $C_{0,DOPE}$ (= 1/(−30.2) Å^{-1}) at [Ca^{2+}] = 0 mM and 20 °C, a condition

This journal is © The Royal Society of Chemistry 2015

Published on 16 April 2015. Downloaded by National Center for High-Performance Computing on 15/05/2015 02:18:35.

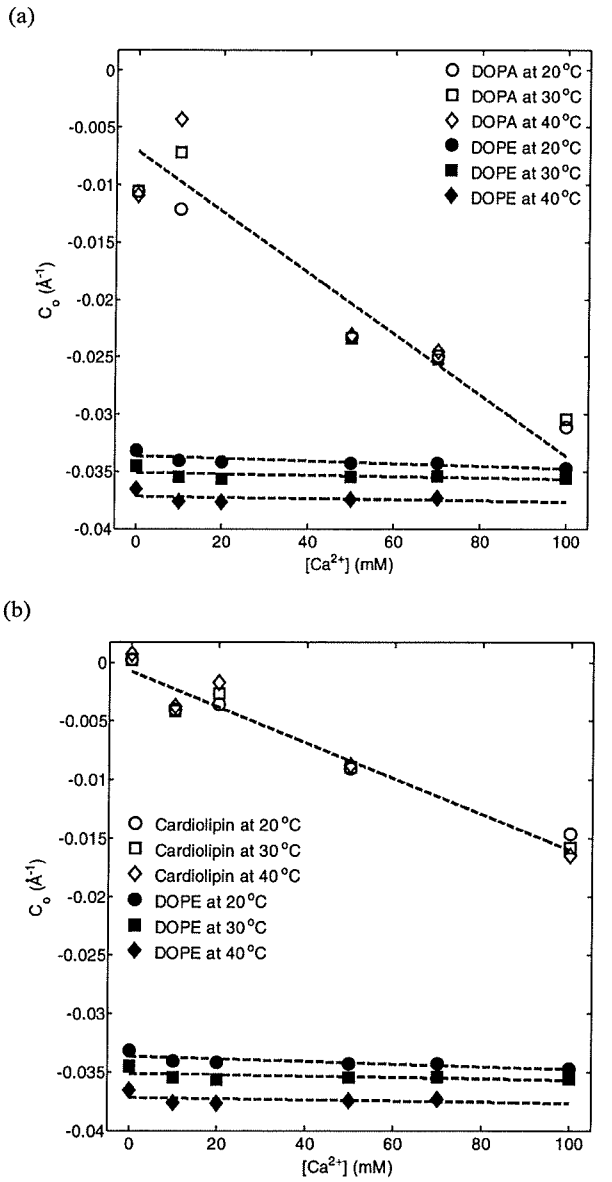

Fig. 5 $C_{0,DOPA}$ (a) and $C_{0,cardiolipin}$ (b) as a function of [Ca^{2+}] for different temperatures. The [Ca^{2+}] dependence of $C_{0,DOPE}$ is also shown for comparison. The dashed lines are linear fits to the sets of data points. The C_0s of DOPA and cardiolipin were determined through the linear extrapolations as depicted in Fig. 3.

where the H_{II} phase is the sole stable phase for DOPE even when no free hydrocarbon is added to relieve the packing frustration.[4,29] On the contrary, the change in [Ca^{2+}] of the same extent only drives $C_{0,cardiolipin}$ to a medium value of 1/(−68.5) Å^{-1}, less than half of the magnitudes of the $C_{0,DOPA}$ or $C_{0,DOPE}$ for the same condition (Table 1). Given the sequence, $L_\alpha \rightarrow Q_{II} \rightarrow H_{II}$, in the order of increasing total curvature magnitude,[40,41] it is tempting to claim that DOPA and cardiolipin in the excess water conditions turn their phase preferences from the L_α phase to the H_{II} and Q_{II} phases, respectively, when [Ca^{2+}] is varied from 0 mM to 100 mM; the case regarding cardiolipin seems particularly valid, given that the packing frustration of a Q_{II} phase is nearly negligible.[42] (Q_{II} phases are a family of type II structures where the midplane of a bilayer is draped on the infinite periodic minimal surface and separates two intertwined but independent water layers; see ref. 40 for a review.) Nevertheless, a scrutiny of the conditions where a Q_{II} phase can form is still warranted to verify the cardiolipin part of the claim. Based on the energetics consideration, Siegel and Kozlov indicated that for a Q_{II} phase to be energetically preferred over the L_α and H_{II} phases, the following condition must be satisfied:[43]

$$\frac{K_G}{K} > 2\delta \times C_0, \qquad (4)$$

where δ is the distance between the midplane of the Q_{II} bilayer and the neutral plane (a dividing surface within the monolayer where bending and stretching are energetically independent); and K_G/K is the ratio of the Gaussian to the bending moduli for a monolayer. Substituting the $C_{0,cardiolipin}$ value obtained here for 20 °C and [Ca^{2+}] = 100 mM into eqn (4) leads to:

$$\frac{K_G}{K} > 2\delta \times C_{0,cardiolipin} = 2 \times 13 \times \frac{-1}{68.5} = -0.38 \qquad (5)$$

with δ = 13 Å adopted from ref. 43. This means the K_G/K of the cardiolipin monolayer at 20 °C and [Ca^{2+}] = 100 mM must be larger than −0.38 if the preferred phase of cardiolipin in this condition is a Q_{II} phase. However, all the currently known values of K_G/K, determined experimentally or computationally for various lipids, including those favoring the Q_{II} phases, are far smaller than −0.38 (see ref. 44 and the references therein). (Eqn (5) will become $K_G/K > -0.48$, if the $C_{0,cardiolipin}$ is defined against the neutral plane; again, the known values of K_G/K cited above are still far smaller than −0.48.) Therefore, it is very unlikely that a Q_{II} phase is the energetically favored phase for cardiolipin at 20 °C and [Ca^{2+}] = 100 mM under excess water condition, even though the $C_{0,cardiolipin}$ magnitude has increased considerably upon varying [Ca^{2+}] to 100 mM. Indeed, to the best of our knowledge, cations are not known for promoting the formation of a Q_{II} phase for pure cardiolipin in the excess water conditions (*e.g.*, see ref. 45 and 46).

In the absence of free Ca^{2+}, the $C_{0,DOPA}$ at 20 °C is 1/(−94.3) Å^{-1}. This value is in between the ones reported in ref. 5 for DOPA in an unbuffered aqueous medium (*i.e.*, $C_{0,DOPA}$ = 1/(−130) Å^{-1} at 22 °C) and in the buffered solution (pH = 7.0) containing [NaCl] = 150 mM (*i.e.*, $C_{0,DOPA}$ = 1/(−46) Å^{-1} at 22 °C). This discrepancy may arise from the difference in the conditions of the aqueous medium. This reveals the substantial influence on anionic phospholipids of the solvent condition, particularly the ionic strength and acidity.

The temperature dependencies of the C_0s of DOPA and 18 : 1 (9Z) cardiolipin

The temperature effect on $C_{0,DOPA}$ and $C_{0,cardiolipin}$ is summarized in Fig. 4. Surprisingly, $C_{0,DOPA}$ and $C_{0,cardiolipin}$ are essentially independent of temperature at nearly each of the [Ca^{2+}]s examined. It is widely known that elevating temperature can increase the magnitude of a negative C_0 because of the enhanced

Published on 16 April 2015. Downloaded by National Center for High-Performance Computing on 15/05/2015 02:18:35.

splaying of the hydrocarbon chains at higher temperatures, as demonstrated here by the temperature dependence of $C_{0,DOPE}$. The lack of a significant influence on $C_{0,DOPA}$ and $C_{0,cardiolipin}$ of temperature, at least in the temperature range investigated here, may indicate the presence of another factor that compromises the greater hydrocarbon chain splaying at higher temperatures, leaving the C_0s unchanged. As will be discussed in the following section, this phenomenon is likely to involve the electrostatic repulsions between the headgroups of the two phospholipids. It is not yet clear whether this weak sensitivity to temperature is a general feature among anionic phospholipids or only specific to DOPA and 18:1 (9*Z*) cardiolipin. More studies are still needed.

It must be emphasized again that any one of the C_0-temperature correlations (*i.e.*, any set of data points fitted with a dashed line) for DOPA (or cardiolipin) in Fig. 4 was derived from a series of DOPE–DOPA (or DOPE–cardiolipin) mixtures, each with a fixed molar ratio. Hence, every data point was based on many independent samples rather than on one single sample (see sample preparation).

Discussions

Electric charge density as the dominating factor in determining the relaxed molecular shapes and phase preferences of DOPA and 18:1 (9*Z*) cardiolipin

The phase preference of a phospholipid is dictated by its relaxed molecular shape, or more specifically by the relative sizes of the headgroup and the hydrocarbon chain region under the given conditions. Comparing DOPA and cardiolipin in this context can be intriguing and informative. The relationship between DOPA and cardiolipin is not unlike the one between a surfactant and its corresponding gemini surfactant. A cardiolipin molecule therefore carries two more hydrocarbon chains and nominally one more net electric charge on its headgroup than does a DOPA molecule. In general, phospholipids with bulkier hydrocarbon chain regions have higher tendencies of forming type II structures. This is attested by comparing DOPA and lyso-DOPA (*i.e.*, the DOPA with one of the two hydrocarbon chains hydrolyzed), which have a $C_0 < 0$ and $C_0 > 0$, respectively.[5] Therefore, the quadruple-chained configuration shall drive cardiolipin to grow more cone-shaped and make type II structures more favorable to cardiolipin than to DOPA. Nevertheless, the additional net charge on cardiolipin is also expected to further enlarge its headgroup region (presumably due to the strengthening of the electrostatic repulsion by the additional headgroup charge) and shift its phase preference more toward the lamellar structures, as manifested in the C_0–$[Ca^{2+}]$ correlations (or equivalently, the correlations between C_0 and the strength of the inter-headgroup repulsion, which was modulated by varying $[Ca^{2+}]$) shown in Fig. 5. Overall, were it not for the difference in charge density between the two phospholipids, cardiolipin would have undoubtedly been a strong nonlamellar-favoring phospholipid compared to DOPA, given its bulky hydrocarbon chain region. It is then interesting to ask: which one of the two opposing factors, adding hydrocarbon chains or increasing charge density, would prevail in defining the relaxed molecular shape and consequently the phase preference of cardiolipin relative to DOPA? Based on the very fact that $C_{0,DOPA}$ is more negative than $C_{0,cardiolipin}$ (see Table 1), it is understood that the increase in charge density per molecule is the dominating factor in defining the relaxed molecular shape and the phase preference. The positivity of $C_{0,cardiolipin}$ at $[Ca^{2+}] = 0$ mM even suggests that the effect of escalating charge density is so potent that cardiolipin is more inclined to forming a type I structure than to forming a type II phase, and that the headgroup region of cardiolipin is larger than its bulky hydrocarbon chain region. This claim is supported by the fact that the L_α phase is the preferred phase for cardiolipin even at $[Ca^{2+}] = 100$ mM (see the last section). Following this reasoning, we further speculate that the charge density per molecule predominates over chain configuration/conformation in defining both $C_{0,DOPA}$ and $C_{0,cardiolipin}$. This speculation is consistent with the temperature independence observed here for $C_{0,DOPA}$ and $C_{0,cardiolipin}$, because the null sensitivity to temperature of the C_0s may indicate the effect of the thermally induced chain splaying being compromised, presumably, by the electrostatic repulsions between the headgroups. The information learned here can be of practical value to designing the materials used in the applications where the self-assembling behavior of lipids are important, such as in the Q_{II}-based drug delivery system for gene therapy.[47]

Our proposition that the prevalence of charge density over chain configuration/conformation makes type II phases less favorable to cardiolipin than to DOPA is consistent with some earlier observations. Similar to Ca^{2+}, H^+ is also expected to screen the headgroup charges and thus weaken the inter-headgroup repulsions. Early NMR and X-ray diffraction studies on the phase behavior of DOPA and bovine heart cardiolipin (this cell extract contains >88% 18:2 (9*Z*,12*Z*) cardiolipin, supposedly having a higher tendency of forming type II structures than the 18:1 (9*Z*) cardiolipin) showed that at 25 °C DOPA could form a pure H_{II} phase at pH $\leq$ 3.7, while for bovine heart cardiolipin, the L_α phase could not be transformed to the H_{II} phase completely even as the acidity was as high as pH = 2.8 at 23 ± 5 °C.[45,48] It seems that our study amounts to one of the few instances where the otherwise qualitative observations on phase behavior can be described quantitatively and explained mechanistically. However, it is emphasized that we do not rule out the possibilities where other factors (*e.g.*, the difference in hydration, the presence/absence of the hydrogen-bond network or the "pure" headgroup size when the charge is neutralized) dictate $C_{0,cardiolipin}$ collectively with charge density.

The biological implications of the $[Ca^{2+}]$ dependencies of the C_0s of DOPA and 18:1 (9*Z*) cardiolipin

A biomembrane may maintain its C_0 within a certain range of nonzero values in the need of regulating the conformations and functioning of membrane proteins, even though a biomembrane is usually in the lamellar structure;[8,10–12] the C_0 of a biomembrane was even shown to differ in the different stages of the cell cycle.[51] It is known from our C_0 measurements that DOPA and

 This journal is © The Royal Society of Chemistry 2015

Published on 16 April 2015. Downloaded by National Center for High-Performance Computing on 15/05/2015 02:18:35.

cardiolipin collectively display a wide range of C_0s that are adaptive to the aqueous conditions. Cells may exploit this rich repertoire of C_0s to regulate protein conformations and functioning in coordination with the local aqueous conditions (*e.g.*, local $[Ca^{2+}]$, $[Na^+]$ or $[H^+]$; living organisms are in the non-equilibrium state, and the conditions can vary significantly with time and with intracellular locations).

The differential responses to the $[Ca^{2+}]$ variation (or, in general, to a change in conditions regarding an electrically charged object) of $C_{0,DOPA}$ and $C_{0,cardiolipin}$ also have their biological implications, the one relevant to $C_{0,DOPA}$ being correlated with the intracellular transport concerning the vesicle fissions from the Golgi-apparatus. Local adjustment of the C_0 of a biomembrane is important to the vesicle transport. Local membrane bending and distortion, which involve changes in the curvature of a biomembrane, are a prominent feature of membrane fissions;[52,53] carrying out the budding process of fission is even known to require the acquisition of negative C_0s by a biomembrane.[54] The C_0 modulation for the vesicle transport may be regulated with PA, a key lipid to this intracellular transport,[52,53,55–57] through the interconversion of three PA-related lipids, namely PA, lyso-PA and DAG (diacylglycerol, the PA with the headgroup de-phosphorylated).[57] Indeed, while DAG is crucial to the bud formation and to stabilizing the neck of a budding vesicle, converting DAG to PA or lyso-PA is required for the formation of the hemi-fission intermediate and for the completion of the fission process.[52–54,58] This enzymes-catalyzed conversion of DAG → PA → lyso- PA incurs local changes to the C_0 of a biomembrane, from a negative value, through a nearly zero value, to a positive value.[5,59] It has been shown that a lack of the negative C_0s endowed by the PA → DAG conversion constrained the bud formation on a biomembrane.[54] Therefore, cells may arrange the enzymes near the budding sites of a biomembrane and interconvert the three lipid species to adjust the C_0 of the biomembrane to satisfy the diverse needs in the C_0 value at different fission stages (Fig. 6, upper panel). Alternatively, based on the strong $[Ca^{2+}]$-dependence observed here for $C_{0,DOPA}$, we raise the possibility that this adaptive modulation of C_0 can also be achieved through another mechanism, in which cells deploy the calcium ion channels (and/or proton pumps) to control the local $[Ca^{2+}]$ (and/or $[H^+]$) near the budding sites and exploit the strong $[Ca^{2+}]$ (presumably, and/or $[H^+]$) sensitivity of $C_{0,DOPA}$ to locally regulate the C_0 of the biomembrane between a nearly zero to a strongly negative value; the need of interconverting PA and DAG is thus skirted (Fig. 6, lower panel). It must be noted that the PA ↔ DAG interconversion and the Ca^{2+}- (and/or H^+-) mediated mechanisms or even other yet-to-be recognized mechanisms can coexist in a cell without mutually excluding one another, as living organisms are known to exploit redundancy to hedge the risks of the malfunctioning of one machinery.

On the other hand, the insensitivity to the $[Ca^{2+}]$ variation, or to a change in conditions regarding a charged object in general, of the phase preference of cardiolipin may provide the cardiolipin-rich biomembranes with the features much needed for carrying out the cellular functions of cardiolipin. In eukaryotes, cardiolipin is nearly exclusively found in the inner membranes of mitochondria,[60] where many vital events, such as intracellular calcium storage, oxidative phosphorylation and apoptosis, take place.[61,62] Given its close relation with the mitochondrion, cardiolipin is naturally expected to play an important role in mitochondrial functioning.[63] To the mitochondrial function of calcium storage, the weak $[Ca^{2+}]$ dependence of the phase preference of cardiolipin can be beneficial: it attenuates the usually strong nonlamellar-forming propensities of anionic phospholipids at high local $[Ca^{2+}]$ (retaining high local $[Ca^{2+}]$ is important to mitochondrial functioning, as reviewed in ref. 17 and 18). This in turn maintains the integrity of the lamellar bilayer structure for the cardiolipin-rich mitochondrial inner membranes. Other mitochondrial functions that may be benefitted from the low $[Ca^{2+}]$ dependence of cardiolipin are oxidative phosphorylation and apoptosis. Properly performing the two functions requires a positively charged protein, cytochrome *c*.

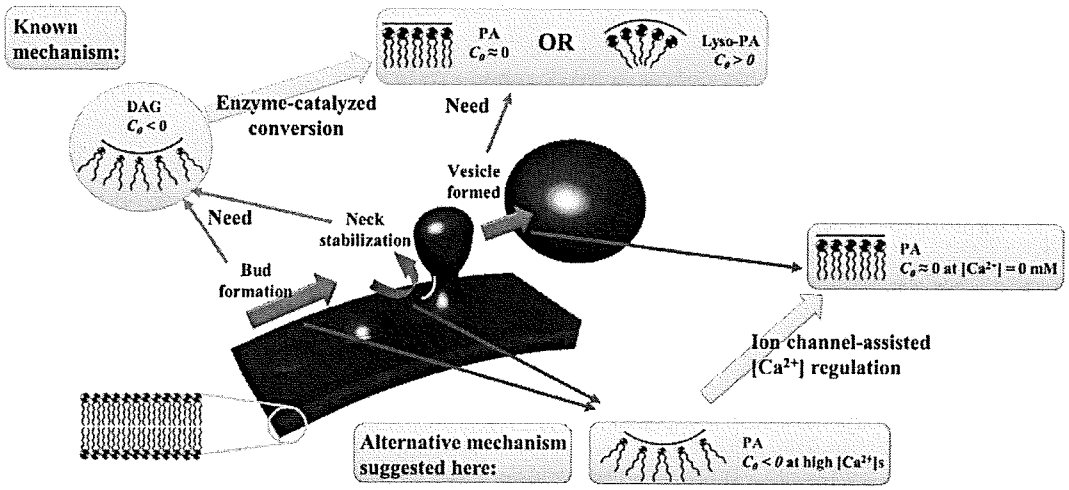

Fig. 6 Mechanisms of the C_0 regulation for the vesicle fission of intracellular transport: (upper) the known mechanism; (lower) the mechanism suggested here.

Published on 16 April 2015. Downloaded by National Center for High-Performance Computing on 15/05/2015 02:18:35.

This protein is normally localized onto the inner membrane of a mitochondrion, through its electrostatic interaction specifically with cardiolipin.[64] Like Ca^{2+}, the positive charges carried by proteins/peptides also screen the headgroup charges of anionic phospholipids and weaken the inter-headgroup repulsion, which intensifies their tendencies of forming type II structures.[10,65] Accordingly, we speculate that were it not for the insensitivity of the phase preference of cardiolipin to the disruption of the inter-headgroup repulsion by charged objects, the binding of cytochrome *c* to cardiolipin would have jeopardized the structural integrity of the mitochondrial inner membrane.

These biological implications relevant to cardiolipin may provide a clue to a long-lasting puzzle: Why does cardiolipin have such a unique chemical structure, with one cardiolipin molecule carrying four hydrocarbon chains and nominally two net charges, rather than two hydrocarbon chains and one net charge as for other common anionic phospholipids? Based on our data and discussions above, we argue that whereas the high charge density of cardiolipin endows the cardiolipin-rich biomembranes with the structural stability against charged objects (*e.g.*, Ca^{2+} and cytochrome *c*), cardiolipin's tendency of acquiring a strongly positive C_0 driven by this high charge density is counterbalanced by its four hydrocarbon chains; failure of averting a strongly positive C_0 could structurally destabilize biomembranes as well, as lipids with positive C_0s were shown to increase the membrane permeation of mitochondria during apoptosis.[66] As a result, lack of either of the two molecular characteristics of cardiolipin can be detrimental to the structural integrity of the mitochondrial inner membranes, which are rich in cardiolipin, and to carrying out the cellular functions of cardiolipin, such as securing cytochrome *c* onto the inner membranes of mitochondria (Fig. 7).

It has to be noted that the spatial-averaged $[Ca^{2+}]$s rarely reach the millimolar level in the cytosol of a cell or in the matrices of its cellular organelles (with the dimensions of μm or larger).[19,69] This fact appears to invalidate the biological implications presented above. Nevertheless, the non-equilibrium nature of a living cell may paint a very different picture when the concerned spatial dimension is down to nanometers (the scale that is relevant to the membrane deformations discussed here, such as the neck formation of vesicles[71]); the local $[Ca^{2+}]$s in this scale could be very high, particularly in the regions next to the calcium ion channels, and reach the levels where our arguments apply. Moreover, Ca^{2+} is not the only charged objects present in cells; Na^+, K^+ and Mg^{2+}, to name a few, also have significant presences *in vivo* (*e.g.*, $[K^+]$ is even as high as 150 mM inside cells). These ions are also charged objects capable of disrupting the inter-headgroup repulsions of PA and cardiolipin synergistically with Ca^{2+}. All these considerations would strengthen the applicability of our propositions above. (For cardiolipin, cytochrome *c* is yet another potent charged object, which is multivalent and can strongly affect the inter-headgroup repulsion of the phospholipid.)

The mechanism of the cation-induced $L_\alpha \rightarrow H_{II}$ phase transitions for PE

Cations are known to induce/stabilize the H_{II} phase for some zwitterionic phospholipids such as PE: the presence of ~1.5 mM La^{3+} or ~50 mM Ca^{2+} is sufficient to promote the formation of the H_{II} phase at 20 °C for the otherwise lamellar-favoring phospholipid, POPE (*i.e.*, 16:0/18:1 PE);[67] and the $L_\alpha \rightarrow H_{II}$ transition temperature for DEPE (*i.e.*, 18:1 (9*E*) PE) can be depressed noticeably with even a minor introduction of La^{3+} in hundreds of nM or of Ca^{2+} in tens of mM.[38] One may promptly expect that the strong effects of the cations are related, at least partially, to the changes in C_0. Nevertheless, our measurement indicates a nearly negligible $[Ca^{2+}]$ dependence of $C_{0,DOPE}$ (Fig. 5). This observation agrees with the findings of earlier studies in which the H_{II} lattice spacing of POPE was found to be independent of $[La^{3+}]$ and barely decrease with increasing $[Ca^{2+}]$,[67] and $C_{0,DOPE}$ was observed to change only marginally from $1/(-27 \pm 1)$ Å^{-1} to $1/(-23 \pm 1)$ Å^{-1} when $[Na^+]$ was varied from 0 mM to 150 mM.[5] Although the magnitude of $C_{0,DOPE}$ grows slightly larger with $[Ca^{2+}]$ (Fig. 5), such small variations are unable to account for the considerable change of the PE phase behavior observed in the cited studies. The situation is further complicated by the fact that the binding affinity of Ca^{2+} is markedly lower to PE than to several PC species.[39] Although the low binding affinity of Ca^{2+} to PE is consistent with the low $[Ca^{2+}]$ dependence of $C_{0,DOPE}$, a more challenging question emerges immediately: how can Ca^{2+} shift the phase preference of PE so drastically, even though its binding affinity to PE is low and its effect on C_0 is nearly negligible? Here, we resort to a mechanism proposed in ref. 67 to address this issue.

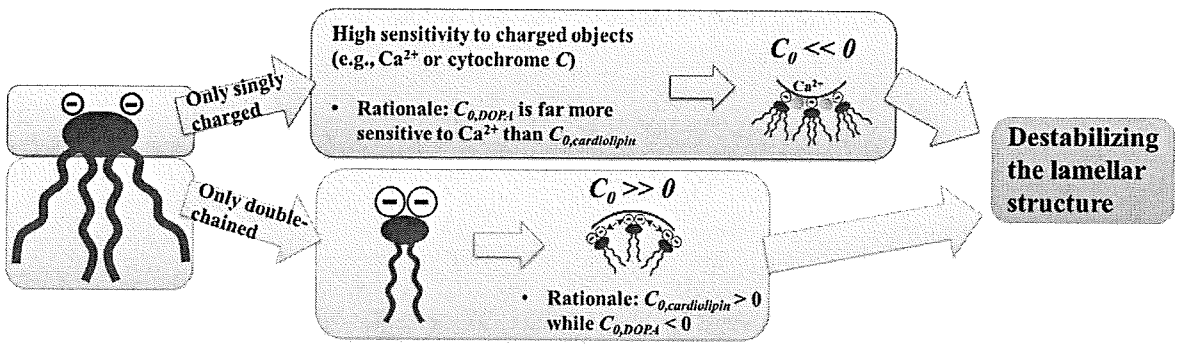

Fig. 7 Biological significance of the molecular characteristics (*i.e.*, the doubly charged headgroup and quadruple chained tails) of cardiolipin.

This journal is © The Royal Society of Chemistry 2015

Published on 16 April 2015. Downloaded by National Center for High-Performance Computing on 15/05/2015 02:18:35.

Minimizing the elastic stress and avoiding the packing frustration of the hydrocarbon chains (see Introduction) can be two competing energetic demands that dictate the phase behavior of a phospholipid, since the elastic stress and packing frustration favor and hinder the formation of a type II structure, respectively, in many occasions. In addition to elevating the magnitude of a negative C_0, the $L_\alpha \rightarrow H_{II}$ transition can therefore be promoted by lessening the packing frustration of the H_{II} phase. Accordingly, the cation-induced $L_\alpha \rightarrow H_{II}$ transition for PE is likely to involve the lessening of the packing frustration rather than the increasing of the C_0 magnitude. Earlier studies may illuminate how the packing frustration can be lessened in this case. Through X-ray diffraction experiments for a series of PC–DOPE mixtures, a study found that the $L_\alpha \rightarrow H_{II}$ transition temperature was depressed when DOPC in the mixture was replaced with its longer-chain counterparts (*i.e.*, the PC species with the chains longer than those of both DOPC and DOPE).[49] The authors attributed the depression in the transition temperature to the partial relief of the packing frustration, which was likely to result from the filling of the interstices of the H_{II} phase (Fig. 1b) by the longer chains of the PC. Furthermore, it was reported that addition of La^{3+}, Ca^{2+}, or Na^+ could also elevate the main transition temperatures of PE and PC.[50,67] This implies that the cations elongate the hydrocarbon chains and in consequence make the chains packed more ordered and closely, which in turn results in the higher main transition temperatures. A more direct experimental evidence was even presented to confirm the chain-elongation and chain-ordering effects of Ca^{2+} and Na^{2+} for POPC.[50] Altogether, it is likely that Ca^{2+} elongates the hydrocarbon chains of the very DOPE molecules that adsorb it, and the elongated chains fill the interstices of the H_{II} phase once the structure is formed, thus lessening the packing frustration and promoting the $L_\alpha \rightarrow H_{II}$ transition, as suggested in ref. 67. In this scenario, a relatively small amount of the Ca^{2+}-adsorbing phospholipid molecules are sufficient to promote the $L_\alpha \rightarrow H_{II}$ transition since, according to our calculations based on ref. 12, only a small fraction of the hydrocarbon chains (around 14%) are under the packing stress. On the contrary, the influence of Ca^{2+} on $C_{0,DOPE}$, if any, is limited by the low binding affinity of Ca^{2+} to PE. This is because C_0 is a collective property of the supramolecular structure formed by a phospholipid, and a majority of the composing molecules must be affected by the cation before its effect on C_0 is detectable.

We caution readers that even with its apparent applicability in explaining the cation-induced $L_\alpha \rightarrow H_{II}$ transition for PE, this mechanism remains highly speculative. More studies are still desired to confirm its validity.

Conclusions

In this study, we measured C_0 under various conditions for DOPE, DOPA and cardiolipin, which carried an identical type of hydrocarbon chains but had different headgroup charge densities. The comparison of the obtained C_0s revealed the importance of molecular charge density in shaping the phase behavior of the phospholipids: $C_{0,DOPA}$ varied with $[Ca^{2+}]$ more strongly than $C_{0,cardiolipin}$, while $C_{0,DOPE}$ is independent of $[Ca^{2+}]$; and the phase preferences of DOPA and cardiolipin were shifted to the H_{II} phase and remained on the L_α phase, respectively, when $[Ca^{2+}]$ rose from 0 mM to 100 mM. Moreover, molecular charge density was concluded to even prevail over chain configuration/conformation in dictating the phase preferences of DOPA and cardiolipin, given the observations that $|C_{0,DOPA}| > |C_{0,cardiolipin}|$, $C_{0,cardiolipin} > 0$ while $C_{0,DOPA} < 0$ and the phase behavior described above. This dominance of charge density also explained the temperature independence observed here for $C_{0,DOPA}$ and $C_{0,cardiolipin}$. The difference in the strength of the inter-headgroup repulsion underlies all of these observations and conclusions, and is crucial to the phase behavior of the anionic phospholipids.

We further consider modulating the strength of the inter-headgroup repulsion being also biologically relevant. Cells, we argue, may use the differential sensitivities to electrically charged objects (*e.g.*, Ca^{2+} and cytochrome *c*), which tune the strength of the inter-headgroup repulsion, of the phase preferences of DOPA and cardiolipin to carry out their respective cellular functions: The local adjustment of C_0 catering to the needs in different vesicle-fission stages can be achieved by exploiting the high $[Ca^{2+}]$ (or conditions regarding other charged objects, such as $[H^+]$) sensitivity of $C_{0,DOPA}$, while the stability against charged objects of the phase preference of cardiolipin ensures the structural integrity of the cardiolipin-rich mitochondrial inner membranes upon binding of cytochrome *c* and the rise of the local $[Ca^{2+}]$. Moreover, we suggest that cardiolipin's tendency of acquiring a strongly positive C_0 driven by its high charge density, which endows the structural stability described above, is counteracted by its quadruple-chained tails. All these point to the biological relevance of the unique molecular feature of cardiolipin.

Interestingly, electrically charged objects do not affect the phase behavior of electrically charged phospholipids only; earlier studies have shown that cations could also induce the $L_\alpha \rightarrow H_{II}$ transition for some zwitterionic phospholipids, such as DEPE and POPE. Given that $C_{0,DOPE}$ demonstrated a negligible dependence on $[Ca^{2+}]$ here, we conclude that this cation-induced phase transition may be enabled by the cation-induced stretching of the hydrocarbon chains, which relieves the packing frustration.

Acknowledgements

This study is supported by the Ministry of Science and Technology of Taiwan (Grant no.: MOST 103-2221-E-008-113) and by National Central University. We thank the scientific and technical supports from the staff scientists of Beamlines BL13A and BL23A of NSRRC.

Notes and references

1 L. V. Chernomordik and M. M. Kozlov, *Nat. Struct. Mol. Biol.*, 2008, **15**, 675–683.
2 R. Jahn, T. Lang and T. C. Südhof, *Cell*, 2003, **112**, 519–533.

Published on 16 April 2015. Downloaded by National Center for High-Performance Computing on 15/05/2015 02:18:35.

3 B. Kollmitzer, P. Heftberger, M. Rappolt and G. Pabst, *Soft Matter*, 2013, **9**, 10877–10884.
4 M. W. Tate and S. M. Gruner, *Biochemistry*, 1989, **28**, 4245–4253.
5 E. E. Kooijman, V. Chupin, N. L. Fuller, M. M. Kozlov, B. de Kruijff, K. N. J. Burger and P. R. Rand, *Biochemistry*, 2005, **44**, 2097–2102.
6 T.-Y. D. Tang, N. J. Brooks, C. Jeworrek, O. Ces, N. J. Terrill, R. Winter, R. H. Templer and J. M. Seddon, *Langmuir*, 2012, **28**, 13018–13024.
7 R. Winter, J. Erbes, R. H. Templer, J. M. Seddon, A. Syrykh, N. A. Warrender and G. Rappe, *Phys. Chem. Chem. Phys.*, 1999, **1**, 887–893.
8 D. Marsh, *Biophys. J.*, 2007, **93**, 3884–3899.
9 S. M. Gruner, M. W. Tate, G. L. Kirk, P. T. C. So, D. C. Turner, D. T. Keane, C. P. S. Tilcock and P. R. Cullis, *Biochemistry*, 1988, **27**, 2853–2866.
10 D. Koller and K. Lohner, *Biochim. Biophys. Acta*, 2014, **1838**, 2250–2259.
11 M. Wikström, A. A. Kelly, A. Georgiev, H. M. Eriksson, M. R. Klement, M. Bogdanov, W. Dowhan and Å. Wieslander, *J. Biol. Chem.*, 2009, **284**, 954–965.
12 S. M. Gruner, *Proc. Natl. Acad. Sci. U. S. A.*, 1985, **82**, 3665–3669.
13 S. L. Keller, S. M. Bezrukov, S. M. Gruner, M. W. Tate, I. Vodyanoy and V. A. Parsegian, *Biophys. J.*, 1993, **65**, 23–27.
14 P. Urbina, M. Flores-Díaz, A. Alape-Girón, A. Alonso and F. M. Goñi, *Biochim. Biophys. Acta*, 2011, **1808**, 279–286.
15 E. Strandberg, D. Tiltak, S. Ehni, P. Wadhwani and A. S. Ulrich, *Biochim. Biophys. Acta*, 2012, **1818**, 1764–1776.
16 T. K. Rostovtseva, P. A. Gurnev, M.-Y. Chen and S. M. Bezrukov, *J. Biol. Chem.*, 2012, **287**, 29589–29598.
17 D. E. Clapham, *Cell*, 2007, **131**, 1047–1058.
18 P. Pinton, C. Giorgi, R. Siviero, E. Zecchini and R. Rizzuto, *Oncogene*, 2008, **27**, 6407–6418.
19 M. V. Ivannikov and G. T. Macleod, *Biophys. J.*, 2013, **104**, 2353–2361.
20 A. K. Chouhan, M. V. Ivannikov, Z. Lu, M. Sugimori, R. R. Llinas and G. T. Macleod, *J. Neurosci.*, 2012, **32**, 1233–1243.
21 T. C. Südhof, *Annu. Rev. Neurosci.*, 2004, **27**, 509–547.
22 R. P. Rand, N. L. Fuller, S. M. Gruner and V. A. Parsegian, *Biochemistry*, 1990, **29**, 76–87.
23 G. L. Kirk and S. M. Gruner, *J. Phys.*, 1985, **46**, 761–769.
24 R. P. Rand and V. A. Parsegian, *Biochim. Biophys. Acta*, 1989, **988**, 351–376.
25 R. N. A. H. Lewis and R. N. McElhaney, *Biophys. J.*, 2000, **79**, 1455–1464.
26 Y. S. Tarahovsky, A. L. Arsenault, R. C. MacDonald, T. J. McIntosh and R. M. Epand, *Biophys. J.*, 2000, **79**, 3193–3200.
27 D. C. Turner and S. M. Gruner, *Biochemistry*, 1992, **31**, 1340–1355.
28 B. E. Warren, *X-ray diffraction*, Addison-Wesley Pub. Co., Reading, Mass., 1969.
29 P. E. Harper, D. A. Mannock, R. N. A. H. Lewis, R. N. McElhaney and S. M. Gruner, *Biophys. J.*, 2001, **81**, 2693–2706.
30 M. Rappolt, A. Hodzica, B. Sartoria, M. Ollivonb and P. Laggner, *Chem. Phys. Lipids*, 2008, **154**, 46–55.
31 N. Fuller, C. R. Benatti and R. P. Rand, *Biophys. J.*, 2003, **85**, 1667–1674.
32 D. Marsh, *Chem. Phys. Lipids*, 2011, **164**, 177–183.
33 S. Leikin, M. M. Kozlov, N. L. Fuller and R. P. Rand, *Biophys. J.*, 1996, **71**, 2623–2632.
34 Z. Chen and R. P. Rand, *Biophys. J.*, 1997, **73**, 267–276.
35 T.-Y. D. Tang, A. M. Seddon, C. Jeworrek, R. Winter, O. Ces, J. M. Seddon and R. H. Templer, *Soft Matter*, 2014, **10**, 3009–3015.
36 B. Boulgaropoulos, M. Rappolt, B. Sartori, H. Amenitsch and G. Pabst, *Biophys. J.*, 2012, **102**, 2031–2038.
37 S. H. Alley, O. Ces, M. Barahonaa and R. H. Templer, *Chem. Phys. Lipids*, 2008, **154**, 64–67.
38 F. Hwang, D.-Q. Zhao, J.-W. Chen, X.-H. Chen and J.-Z. Ni, *Chem. Phys. Lipids*, 1996, **82**, 73–77.
39 X. L. R. Iraolagoitia and M. F. Martini, *Colloids Surf., B*, 2010, **76**, 215–220.
40 G. C. Shearman, O. Ces, R. H. Templer and J. M. Seddon, *J. Phys.: Condens. Matter*, 2006, **18**, S1105–S1124.
41 J. M. Seddon, J. Robins, T. Gulik-Krzywicki and H. Delacroix, *Phys. Chem. Chem. Phys.*, 2000, **2**, 4485–4493.
42 R. H. Templer, B. J. Khoo and J. M. Seddon, *Langmuir*, 1998, **14**, 7427–7434.
43 D. P. Siegel and M. M. Kozlov, *Biophys. J.*, 2004, **87**, 366–374.
44 M. Hu, J. J. Briguglio and M. Deserno, *Biophys. J.*, 2012, **102**, 1403–1410.
45 J. M. Seddon, R. D. Kaye and D. Marsh, *Biochim. Biophys. Acta*, 1983, **734**, 347–352.
46 I. Vasilenko, B. De Kruijff and A. J. Verkleij, *Biochim. Biophys. Acta*, 1982, **684**, 282–286.
47 C. Leal, N. F. Bouxsein, K. K. Ewert and C. R. Safinya, *J. Am. Chem. Soc.*, 2010, **132**, 16841–16847.
48 S. B. Farren, M. J. Hope and P. R. Cullis, *Biochem. Biophys. Res. Commun.*, 1983, **111**, 675–682.
49 M. W. Tate and S. M. Gruner, *Biochemistry*, 1987, **26**, 231–236.
50 G. Pabst, A. Hodzic, J. Štrancar, S. Danner, M. Rappolt and P. Laggner, *Biophys. J.*, 2007, **93**, 2688–2696.
51 C. V. Hague, A. D. Postle, G. S. Attard and M. K. Dymond, *Faraday Discuss.*, 2013, **161**, 481–497.
52 F. Campelo and V. Malhotra, *Annu. Rev. Biochem.*, 2012, **81**, 407–427.
53 J.-S. Yang, C. Valente, R. S. Polishchuk, G. Turacchio, E. Layre, D. B. Moody, C. C. Leslie, M. H. Gelb, W. J. Brown, D. Corda, A. Luini and V. W. Hsu, *Nat. Cell Biol.*, 2011, **13**, 996–1003.
54 L. Asp, F. Kartberg, J. Fernandez-Rodriguez, M. Smedh, M. Elsner, F. Laporte, M. Bárcena, K. A. Jansen, J. A. Valentijn, A. J. Koster, J. J. M. Bergeron and T. Nilsson, *Mol. Biol. Cell*, 2009, **20**, 780–790.
55 R. Beck, M. Ravet, F. T. Wieland and D. Cassel, *FEBS Lett.*, 2009, **583**, 2701–2709.
56 L. Yang, V. D. Gordon, D. R. Trinkle, N. W. Schmidt, M. A. Davis, C. DeVries, A. Som, J. E. Cronan, Jr., G. N. Tew and G. C. L. Wong, *Proc. Natl. Acad. Sci. U. S. A.*, 2008, **105**, 20595–20600.
57 T. Shemesh, A. Luini, V. Malhotra, K. N. J. Burger and M. M. Kozlov, *Biophys. J.*, 2003, **85**, 3813–3827.

 This journal is © The Royal Society of Chemistry 2015

Published on 16 April 2015. Downloaded by National Center for High-Performance Computing on 15/05/2015 02:18:35.

58 S. Kavaliauskiene, C. M. Nymark, J. Bergan, R. Simm, T. Sylvänne, H. Simolin, K. Ekroos, T. Skotland and K. Sandvig, *Cell. Mol. Life Sci.*, 2014, **71**, 1097–1116.
59 J. A. Szule, N. L. Fuller and R. P. Rand, *Biophys. J.*, 2002, **83**, 977–984.
60 D. Ardail, J. P. Privat, M. Egret-Charlier, C. Levrat, F. Lerme and P. Louisot, *J. Biol. Chem.*, 1990, **265**, 18797–18802.
61 S. A. Detmer and D. C. Chan, *Nat. Rev. Mol. Cell Biol.*, 2007, **8**, 870–879.
62 C. Schwimmer, M. Rak, L. Lefebvre-Legendre, S. Duvezin-Caubet, G. Plane and J.-P. di Rago1, *Biotechnol. J.*, 2006, **1**, 270–281.
63 T. Joshi, Z. X. Voo, B. Graham, L. Spiccia and L. L. Martin, *Biochim. Biophys. Acta*, 2009, **1848**, 385–391.
64 Y.-L. P. Ow, D. R. Green, Z. Hao and T. W. Mak, *Nat. Rev. Mol. Cell Biol.*, 2008, **9**, 532–542.
65 O. Domenech, G. Francius, P. M. Tulkens, F. Van Bambeke, Y. Dufrêne and M.-P. Mingeot-Leclercq, *Biochim. Biophys. Acta*, 2009, **1788**, 1832–1840.
66 G. Basañez, J. C. Sharpe, J. Galanis, T. B. Brandt, J. M. Hardwick and J. Zimmerberg, *J. Biol. Chem.*, 2002, **277**, 49360–49365.
67 T. Tanaka, S. J. Li, K. Kinoshita and M. Yamazaki, *Biochim. Biophys. Acta*, 2001, **1515**, 189–201.
68 T. Oka, T.-A. Tsuboi, T. Saiki, T. Takahashi, J. Md. Alam and M. Yamazaki, *Langmuir*, 2014, **30**, 8131–8140.
69 M. Montero, M. T. Alonso, E. Carnicero, I. Cuchillo-Ibáñez, A. Albillos, A. G. García, J. García-Sancho and J. Alvarez, *Nat. Cell Biol.*, 2000, **2**, 57–61.
70 M. M. Kozlov and M. Winterhalter, *J. Phys. II*, 1991, **1**, 1085–1100.
71 H. T. McMahon and J. L. Gallop, *Nature*, 2005, **438**, 590–596.